Transport properties of bottomed mesons in a hot mesonic gas

Luciano M. Abreu[1], Daniel Cabrera[2], and Juan M. Torres-Rincon[3]
[1] *Instituto de Física, Universidade Federal da Bahia, 40210-340, Salvador, BA, Brazil*
[2] *Departamento de Física Teórica II, Universidad Complutense, 28040 Madrid, Spain and*
[3] *Departamento de Física Teórica I, Universidad Complutense, 28040 Madrid, Spain*

In this work we evaluate the B-meson drag and diffusion coefficients in a hot medium constituted of light mesons (π, K, $\bar{K}$ and η). We treat the B-meson and B^*-meson interaction with pseudo-Goldstone bosons in chiral perturbation theory at next-to-leading order within the constraints from heavy quark symmetry, and employ standard unitarization techniques of NLO amplitudes in order to account for dynamically generated resonances (leading to a more efficient heavy-flavor diffusion) and thus reach higher temperatures. We estimate individual meson contributions from the gas to the transport coefficients and perform a comparison with other findings in literature. We report a bottom relaxation length of 83 fm at temperature of 150 MeV and for typical momenta of 1 GeV, at which our approach is reliable. Compared to a charm relaxation length of 40 fm in the same conditions, we conclude that the B mesons provide a cleaner probe of the early stages of a heavy-ion collision.

I. INTRODUCTION

The features of matter formed in Heavy Ion Collisions (HICs) have been a subject of great interest in the last decades. In this scenario, heavy–flavored hadrons play an essential role since they carry heavy quarks produced in the early stage of the collisions. Therefore, heavy mesons are interesting probes to understand the evolution of partonic matter since its creation, unlike pions and kaons which can be produced in the thermal medium at later stages.

However, it is worth noticing that the momentum spectra of charmed and bottomed mesons extracted from HICs undergo modifications due to their interactions with the hadron medium, constituted of pions and other particles. In this sense, the diffusion of heavy mesons in an equilibrium hadronic gas must be taken into account, and may be properly studied in the framework of kinetic theory to compute transport coefficients.

Different approaches have been used to study various aspects of this topic [1–6]. In particular, in Ref. [1] heavy quark effective theory (HQET) and chiral perturbation theory (ChPT) have been employed, focusing on the lowest possible temperatures. Attempts to reach higher temperatures in the context of charmed mesons close to the crossover to the quark and gluon plasma have been done in Refs. [2, 3]. In addition, in Ref. [6] the transport coefficients of B-mesons have been obtained with the use of scattering lengths as dynamical input.

In our recent work [4] the transport coefficients of charmed mesons in a hot pion gas were computed, exploiting ChPT at next-to-leading order (NLO) and employing standard unitarization as guiding principle to reach higher temperatures and account for the contribution of resonant channels. Thus, a natural question arises about the application of this approach to bottomed mesons, which would allow a comparison with existing literature and, hence, a better comprehension of this issue.

In the present work we extend the framework used in [4] to evaluate the B-meson drag and diffusion coefficients in a hot mesonic gas, including pions, kaons and η mesons, with special attention to the contribution of the heavier states with respect to the pion gas. We perform a detailed analysis of the temperature and momentum dependence of these coefficients as well as their static limit (vanishing heavy-meson momentum) and scaling properties with the heavy-meson mass.

The organization of this paper is as follows. In Sec. II, we introduce the transport coefficients and the chiral Lagrangian density that describes the interactions between B-mesons and light mesons. Afterwards, Sec. III is devoted to obtain the unitarized scattering amplitude and fit the relevant free constants to available data. The transport coefficients are evaluated and analyzed in detail in Sec. IV for a pure pion gas. A pertinent discussion of the role of unitarization of scattering amplitudes in heavy-quark diffusion is also contained in this section. The modifications in the transport coefficients due to inclusion of kaons and η mesons in the thermal bath are studied in Sec. V. A summary and concluding remarks are given in Sec. VI.

II. FORMALISM

A. Transport coefficients

We evaluate the transport coefficients of stable B-mesons propagating through a hot mesonic gas by using the scattering amplitudes obtained from chiral perturbation theory, taking into account unitarity and heavy-quark symmetry. We assume that the density of pseudoscalar (B) and vector (B^*) bottomed mesons is very small, so we will neglect collisions among bottomed mesons themselves and concentrate only on their interaction with the light meson gas in thermal equilibrium.

Following the assumptions made in Ref. [4], the momentum-space distribution of bottomed mesons must relax via the Fokker-Planck equation. We choose the mo-

menta of the elastic collision between a meson $B^{(*)}$ and a light meson ϕ as

$$B^{(*)}(\mathbf{p}) + \phi(\mathbf{q}) \to B^{(*)}(\mathbf{p}-\mathbf{k}) + \phi(\mathbf{q}+\mathbf{k}) \ . \quad (1)$$

In this context, the evolution of the momentum distribution of bottomed mesons due to their interaction with the isotropic mesonic gas is fully controlled by the drag (F) and diffusion (Γ_0, Γ_1) coefficients, written as

$$\begin{aligned} F(p^2) &= \int d\mathbf{k}\ w(\mathbf{p},\mathbf{k})\ \frac{k_i p^i}{p^2}\ , \quad (2)\\ \Gamma_0(p^2) &= \frac{1}{4}\int d\mathbf{k}\ w(\mathbf{p},\mathbf{k})\left[\mathbf{k}^2 - \frac{(k_i p^i)^2}{p^2}\right]\ ,\\ \Gamma_1(p^2) &= \frac{1}{2}\int d\mathbf{k}\ w(\mathbf{p},\mathbf{k})\ \frac{(k_i p^i)^2}{p^2}\ , \end{aligned}$$

where $w(\mathbf{p},\mathbf{k})$ denotes the collision rate for a bottomed meson with initial (final) momentum $\mathbf{p}$ ($\mathbf{p}-\mathbf{k}$),

$$w(\mathbf{p},\mathbf{k}) = g_\phi \int \frac{d\mathbf{q}}{(2\pi)^9} f_\phi(\mathbf{q})\left[1+f_\phi(\mathbf{q}+\mathbf{k})\right]\frac{1}{2E_p^B}\frac{1}{2E_q^\phi}\frac{1}{2E_{p-k}^B}\frac{1}{2E_{q+k}^\phi}(2\pi)^4\delta(E_p^B+E_q^\phi-E_{p-k}^B-E_{q+k}^\phi)\sum|\mathcal{M}_{B\phi}(s,t,\chi)|^2. \quad (3)$$

In Eq. (3), $f_\phi(\mathbf{q})$ is the bath's distribution function; $\mathcal{M}_{B\phi}$ stands for the Lorentz invariant B meson - light meson scattering matrix element, g_ϕ is the Goldstone boson isospin degeneracy (i.e. $g_\pi = 3$ for the pion), and χ denotes the possible spin degrees of freedom.

In the next subsection we derive the scattering amplitude $\mathcal{M}$ for bottomed mesons in the light meson medium, necessary to evaluate the three transport coefficients introduced above.

B. Effective Lagrangian for B-meson and light meson interaction

Our task now is to construct the chiral Lagrangian density that describes the interactions between the $J=0$ and $J=1$ B-mesons and light mesons. In this sense, we note that heavy-meson ChPT, described in Refs. [4, 7–9] for the case of charmed mesons, can be applied to the B-meson sector as well.

Let us start by introducing the pseudoscalar Goldstone bosons. They follow the nonlinear realization of the $SU(N_f)_L \times SU(N_f)_R$ chiral symmetry, given in the exponential parametrization

$$U = \exp\left(\frac{\sqrt{2}i\phi}{F}\right), \quad (4)$$

with F being the Goldstone boson decay constant in the chiral limit and ϕ the matrix incorporating the pseudoscalar Goldstone bosons,

$$\phi = \begin{pmatrix} \frac{1}{\sqrt{2}}\pi^0 + \frac{1}{\sqrt{6}}\eta & \pi^+ & K^+ \\ \pi^- & -\frac{1}{\sqrt{2}}\pi^0 + \frac{1}{\sqrt{6}}\eta & K^0 \\ K^- & \bar{K}^0 & -\frac{2}{\sqrt{6}}\eta \end{pmatrix}. \quad (5)$$

Under chiral symmetry, the matrix U is transformed as

$$U \to U' = LUR^\dagger \ , \quad (6)$$

where L and R are global transformations under $SU(3)_L$ and $SU(3)_R$, respectively. The Goldstone boson kinetic term of the effective Lagrangian is explicitly invariant under this symmetry

$$\mathcal{L}^\phi = \frac{F^2}{4}\langle\partial_\mu U^\dagger \partial^\mu U\rangle \ . \quad (7)$$

For convenience, a matrix u is introduced as

$$u = \sqrt{U} \ , \quad (8)$$

and is transformed under chiral symmetry as

$$u \to u' = LuW^\dagger = WuR^\dagger \ , \quad (9)$$

where W is a unitary matrix expressible as a certain combination of L, R and ϕ. The axial and vector fields are constructed as

$$\begin{aligned} \Gamma_\mu &= \frac{1}{2}\left(u^\dagger\partial_\mu u + u\partial_\mu u^\dagger\right)\ ,\\ u_\mu &= i\left(u^\dagger\partial_\mu u - u\partial_\mu u^\dagger\right)\ , \quad (10) \end{aligned}$$

whose transformation laws read

$$\begin{aligned} \Gamma_\mu &\to \Gamma'_\mu = W\Gamma_\mu W^\dagger + W\partial_\mu W^\dagger\\ u_\mu &\to u'_\mu = W u_\mu W^\dagger \ . \quad (11) \end{aligned}$$

Finally, the covariant derivative which acts on the heavy meson field reads

$$\nabla_\mu = \partial_\mu - \Gamma_\mu \ . \tag{12}$$

With these ingredients, the leading-order (LO) chiral Lagrangian $\mathcal{L}^{(1)}$ involving heavy mesons and pseudoscalar Goldstone bosons is given by

$$\begin{aligned}\mathcal{L}^{(1)} \ = \ & \nabla^\mu P \nabla_\mu P^\dagger - m_B^2 P P^\dagger - \nabla^\mu P^{*\nu} \nabla_\mu P^{*\dagger}_\nu \\ & + m_B^2 P^{*\mu} P^{*\dagger}_\mu + ig\left(P^{*\mu} u_\mu P^\dagger - P u^\mu P^{*\dagger}_\mu\right) \\ & + \frac{g}{2m_B}\left(P^*_\mu u_\alpha \nabla_\beta P^{*\dagger}_\nu - \nabla_\beta P^*_\mu u_\alpha P^{*\dagger}_\nu\right)\varepsilon^{\mu\nu\alpha\beta} \ ,\end{aligned} \tag{13}$$

where $P = (B^-, \bar{B}^0, \bar{B}^0_s)$ and $P^*_\mu = (B^{*-}, \bar{B}^{*0}, \bar{B}^{*0}_s)_\mu$ are the SU(3) anti-triplets of spin-zero and spin-one B-mesons with the chiral limit mass m_B and m_{B^*}, respectively. This Lagrangian is indeed invariant under $SU(3)_L \times SU(3)_R$ symmetry. The NLO chiral Lagrangian $\mathcal{L}^{(2)}$ reads

$$\begin{aligned}\mathcal{L}^{(2)} \ = \ & -h_0 P P^\dagger \langle \chi_+ \rangle + h_1 P \chi_+ P^\dagger + h_2 P P^\dagger \langle u^\mu u_\mu \rangle \\ & + h_3 P u^\mu u_\mu P^\dagger + h_4 \nabla_\mu P \nabla_\nu P^\dagger \langle u^\mu u^\nu \rangle \\ & + h_5 \nabla_\mu P \{u^\mu, u^\nu\} \nabla_\nu P^\dagger + \tilde{h}_0 P^{*\mu} P^{*\dagger}_\mu \langle \chi_+ \rangle \\ & - \tilde{h}_1 P^{*\mu} \chi_+ P^{*\dagger}_\mu - \tilde{h}_2 P^{*\mu} P^{*\dagger}_\mu \langle u^\nu u_\nu \rangle \\ & - \tilde{h}_3 P^{*\mu} u^\nu u_\nu P^{*\dagger}_\mu - \tilde{h}_4 \nabla_\mu P^{*\alpha} \nabla_\nu P^{*\dagger}_\alpha \langle u^\mu u^\nu \rangle \\ & - \tilde{h}_5 \nabla_\mu P^{*\alpha} \{u^\mu, u^\nu\} \nabla_\nu P^{*\dagger}_\alpha \ ,\end{aligned} \tag{14}$$

where

$$\chi_+ = u^\dagger \chi u^\dagger + u \chi u \tag{15}$$

and $\chi = \mathrm{diag}(m_\pi^2, m_\pi^2, 2m_K^2 - m_\pi^2)$ being the Goldstone boson mass matrix. The twelve parameters $h_i, \tilde{h}_i (i = 0, ..., 5)$ are the low-energy constants (LECs), to be determined. However, we can make use of some constraints to reduce the set of free LECs. First, it should be noticed that in the limit of large number of colors (N_c) of QCD [10], single-flavor trace interactions are dominant. So, we fix $h_0 = h_2 = h_4 = \tilde{h}_0 = \tilde{h}_2 = \tilde{h}_4 = 0$ henceforth. Besides, by imposing the heavy-quark symmetry, it follows that $\tilde{h}_i \simeq h_i$.

In the following, we use the lowest order of the perturbative expansion of the quantities Γ_μ, u_μ and χ_+ in Eqs. (13) and (14), and construct the scattering matrix of the interaction between the bottomed mesons and the pseudoscalar Goldstone bosons.

III. SCATTERING MATRIX FOR THE BOTTOMED MESON IN THE MESON GAS

A. Scattering matrix elements

With the Lagrangian in Eqs. (13) and (14) we are able to calculate the scattering of pseudoscalar Goldstone bosons ϕ off pseudoscalar B mesons as well as vector B^* mesons. In Fig. 1 we show the tree-level diagrams constructed from the LO and NLO interactions. These include both contact interactions and Born exchanges.

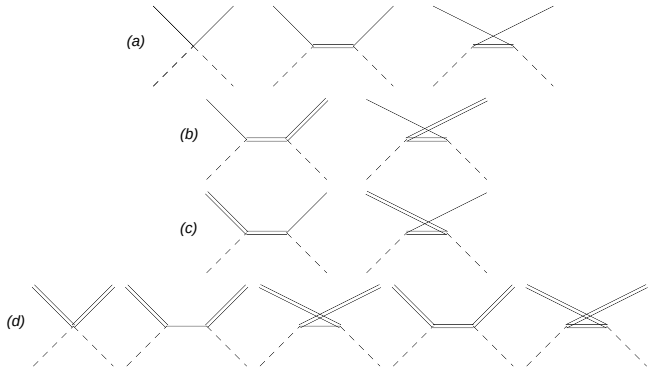

FIG. 1: Tree-level diagrams relevant to the scattering amplitudes for $B^{(*)}\phi \to B^{(*)}\phi$ processes. The solid, double and dashed lines represent the B-mesons, B^*-mesons and Goldstone bosons, respectively.

Note that the Lagrangian density in Eq. (14) has been manifestly constructed maintaining chiral symmetry, that is then broken only carefully in perturbation theory upon expanding in fields and derivatives to construct the LO and NLO chiral amplitudes. However, since the bottomed mesons are heavy fields, the heavy-meson symmetry should be recovered by taking $m_B \to \infty$. We discuss below the implications of this limit in the scattering amplitude.

The spin-changing amplitudes $B^*\phi \to B\phi$ and $B\phi \to B^*\phi$, shown in diagrams (b) and (c) of Fig. 1, should vanish in the limit $m_B \to \infty$, since a collision with a Goldstone boson cannot change the heavy-quark spin, that decouples in this limit. It can be easily proved that indeed these amplitudes are subleading in $1/m_b$ [24].

Turning to the elastic $B\phi$ and $B^*\phi$ amplitudes, displayed in diagrams (a) and (d) of Fig. 1, one finds [4] that the Born exchange terms (proportional to g^2 with an intermediate bottomed meson propagator) are subleading in HQET, and therefore are suppressed by m_B^{-1} with respect to the contact interaction.

Hence, the final amplitude for scattering off a bottom quark in the light meson gas, at NLO in the chiral expansion and LO in the heavy quark expansion, irrespective of whether the heavy quark is in a B or a B^* meson state, is given by

$$\begin{aligned}V \ \simeq \ & \frac{C_0}{2F^2}(s-u) + \frac{2C_1}{F^2}h_1 + \frac{2C_2}{F^2}h_3(p_2\cdot p_4) \\ & + \ \frac{2C_3}{F^2}h_5\left[(p_1\cdot p_2)(p_3\cdot p_4) + (p_1\cdot p_4)(p_2\cdot p_3)\right] \ ,\end{aligned} \tag{16}$$

where C_i $(i = 0, ..., 3)$ are channel-dependent numerical coefficients in isospin basis, as collected in Table I (channels are denoted as $B^{(*)}\phi\,(I)$, with total isospin I).

C_i	$B\pi(\frac{1}{2})$	$B\pi(\frac{3}{2})$	$BK(0)$	$BK(1)$	$B\bar{K}(0)$	$B\bar{K}(1)$	$B\eta(\frac{1}{2})$
C_0	-2	1	-1	1	-2	0	0
C_1	$-m_\pi^2$	$-m_\pi^2$	m_K^2	$-m_K^2$	$-2m_K^2$	0	$-m_\pi^2/3$
C_2	1	1	-1	1	2	0	1/3
C_3	1	1	-1	1	2	0	1/3

TABLE I: Coefficients of the scattering amplitudes for the $B^{(*)}\phi\,(I)$ channels with total isospin I in Eq. (16).

B. Unitarized scattering amplitude

It is well known that ChPT, involving a perturbative expansion up to a certain order, is bound to work properly only at low energies. Particularly, it cannot describe the presence of resonances in specific scattering channels, since a resonance shows up as a pole in the S-matrix complex energy plane. Moreover, the use of ChPT amplitudes at a finite order leads to cross sections which increase monotonically with energy, eventually violating Froissart bounds imposed by the unitarity of the S-matrix. This, in turn, limits the aplicability of the theory in finite-temperature calculations, since the higher the temperature means the more energy available for the two-body interaction.

Imposing unitarity of the scattering amplitudes solves these problems and furthermore accounts for resonances dynamically generated from the LO amplitudes in those channels where the interaction is attractive. In the present case, and motivated by our former experience in the charm sector [4], we can expect to find resonances in the $B^{(*)}\pi\,(1/2)$ and the $B^{(*)}K\,(0)$, $B^{(*)}\bar{K}\,(0)$ S-wave channels, cf. Table I (we briefly review the experimental situation of the B-meson excitation spectrum in Sec. III C). As a resonant interaction implies a more efficient diffusion (and, thus, shorter thermalization times), we believe unitarization of the scattering amplitudes is mandatory in this approach.

Following Refs. [4, 11], using on-shell unitarization via the Bethe-Salpeter equation, the unitarized scalar amplitude T can be written as

$$T(s) = \frac{-V(s)}{1 - V(s)\; G(s)}\;, \tag{17}$$

where $V(s)$ is the S-wave projection of the scattering amplitude in Eq. (16), and $G(s)$ stands for the two-meson loop integral,

$$G(s) = i\int \frac{d^4q}{(2\pi)^4}\frac{1}{(P-q)^2 - m_B^2 + i\epsilon}\frac{1}{q^2 - m_\phi^2 + i\epsilon}\;, \tag{18}$$

where m_ϕ is the mass of the light meson. Employing dimensional regularization, this integral reads

$$\begin{aligned} G(s) \;=\; & \frac{1}{16\pi^2}\left\{ a(\mu) + \ln\frac{m_B^2}{\mu^2} + \frac{m_\phi^2 - m_B^2 + s}{2s}\ln\frac{m_\phi^2}{m_B^2}\right. \\ & + \frac{q}{\sqrt{s}}\left[\ln(s - (m_B^2 - m_\phi^2) + 2q\sqrt{s})\right. \\ & + \ln(s + (m_B^2 - m_\phi^2) + 2q\sqrt{s}) \\ & - \ln(s - (m_B^2 - m_\phi^2) - 2q\sqrt{s}) \\ & \left.\left. - \ln(s + (m_B^2 - m_\phi^2) - 2q\sqrt{s}) - 2\pi i\right]\right\}\;, \end{aligned} \tag{19}$$

where μ is the regularization energy scale, $a(\mu)$ is a subtraction constant which absorbs the scale dependence of the integral, and q is the modulus of the light meson's three-momentum in the CM frame,

$$q = \frac{1}{2\sqrt{s}}\sqrt{[s - (m_\phi + m_B)^2]\,[s - (m_\phi - m_B)^2]}. \tag{20}$$

It is worth mentioning that heavy-meson spin symmetry guarantees the same scattering cross section for both $B\phi$ or $B^*\phi$ channel, and no further spin averaging is needed. Then, we use in the colision rate defined in Eq. (3) the scattering matrix element given by

$$\sum |\mathcal{M}_{B\phi}(s,t,\chi)|^2 = |\overline{T}_{B\phi}|^2\;, \tag{21}$$

where $|\overline{T}_{B\phi}|^2$ is the isospin averaged unitarized amplitude, namely:

$$|\overline{T}_{B\phi}|^2 = \frac{1}{\sum_I (2I+1)}\sum_I (2I+1)|T^I|^2\;, \tag{22}$$

with T^I being derived from Eq. (17) in the total isospin basis.

For the sake of comparison with other systems of interest, we also evaluate the corresponding cross sections in the CM frame,

$$\sigma_{B\phi}(s) = \frac{1}{16\pi s}|\mathcal{M}_{B\phi}|^2\;. \tag{23}$$

C. Free Constants

The only remaining task before proceeding with the calculation of the drag and diffusion coefficients is to determine the free constants of the theory from available data.

At the level of precision that we are working, the pion decay constant in the chiral limit can be approximated by the physical value, $F = 92$ MeV. The values of the meson physical masses that we use are: $m_B = 5279$ MeV, $m_{B^*} = 5325$ MeV, $m_{B_s} = 5366$ MeV, $m_{B_s^*} = 5415$ MeV, $m_\pi = 138$ MeV, $m_K = 496$ MeV and $m_\eta = 548$ MeV [12].

Let us focus on the scattering of pions off B-mesons. We use the renormalization scale $\mu = 1$ GeV, and the scheme is such that the subtraction constant $a(\mu) = -3.47$. Details in the choice of these numbers are given in Appendix A. For this choice of parameters we show in Fig. 2 the squared amplitude, $|T|^2$, for $B\pi$ scattering with isospin $I = 1/2$, keeping only the LO $(s-u)$ term in the elastic amplitude V. This channel, as expected, exhibits a resonant behavior with a peak around $\sqrt{s} \simeq 5530$ MeV, which is in good agreement with the former determinations in [13–15].

Notice that we have only considered the isospin channel $I = 1/2$ in the square amplitude displayed in Fig. 2. The exotic $I = 3/2$ channel is non-resonant in this case and in all situations presented below.

In addition, we compute $|T|^2$ for $B^*\pi$ scattering with $I = 1/2$, just by replacing m_B by m_B^* in $V(B\pi \to B\pi)$. The result is plotted in Fig. 3, where now the peak shows up at $\sqrt{s} \simeq 5580$ MeV, also in agreement with Ref. [16].

Some comments about the theoretical and experimental knowledge of the B-meson spectrum are in order: From heavy quark considerations (confirmed by the well known charmed meson spectrum) one expects a spin 3/2 doublet and a spin 1/2 doublet as first excitations. The former is composed by the states B_1 and B_2, both of which have been observed as the $B_1(5721)^0$ and $B_2^*(5747)$ resonances. These states are narrow, the B_1 state decaying mostly into $B^*\pi$ in D-wave. Therefore, this state does not correspond with the resonance that is generated in our amplitude. On the other hand, other two states B_0 and B_1 are supposed to exist (in analogy with the D_0 and D_1 states for charm) that should be much broader and have not been discovered yet. The latter decays into $B^*\pi$ in S-wave, which would naturally correspond to the state that we find in Fig. 3. As its mass is still not determined experimentally, we can only guess that it is very close to the mass of the other B_1 state, appearing at 5720 MeV. We justify this guess based on the fact that, in the charm sector, the masses of the two D_1 states are nearly the same, and thus we expect the same behavior for the B system provided that heavy quark symmetry works. Many quarks models also predict a similar mass for the two B_1. See Table II for a small review.

Heavy Spin, J^π	D (quark model)	D (experimental)	(M,Γ) MeV	B (quark model)	B (experimental)	(M,Γ) MeV
1/2, 0^+	D_0	$D_0^*(2400)$	2318, 267	$\mathbf{B_0}$	?	?
1/2, 1^+	D_1	$D_1(2430)$	2427, 384	$\mathbf{B_1}$	?	?
3/2, 1^+	D_1	$D_1(2420)^0$	2421, 27	B_1	$B_1(5721)$	5723, ?
3/2, 2^+	D_2	$D_2^*(2460)$	2466, 49	B_2	B_2^* (5747)	5743, 23

TABLE II: List of heavy meson states. Left side: D meson. Right side: B mesons. The two states in bold font are the ones that we obtain in our unitarization scheme. Experimental data taken from [12].

The NLO terms, containing the h_i constants, may be used to improve our results concerning the position of the observed resonances in view of the former discussion. h_1 is fixed by the mass difference between the strange and non-strange B-mesons, as obtained from the chiral Lagrangian $\mathcal{L}^{(2)}$. We have

$$m_{B_s}^2 - m_B^2 = -4h_1(m_K^2 - m_\pi^2), \tag{24}$$

for the pseudoscalar B mesons, and

$$m_{B_s^*}^2 - m_{B^*}^2 = -4h_1(m_K^2 - m_\pi^2), \tag{25}$$

for the vector B mesons. Replacing into these equations the values of the masses introduced above, we get $h_1 = -1.020$ and -1.064 for the scalar and vector cases, respectively. We shall adopt in our computations an average value: $h_1 = -1.042$. We note that the value of h_1 does not yield any relevant changes in the squared amplitudes, since the corresponding term in the NLO amplitude is multiplied by a small m_π^2 constant.

The last free LECs to be estimated are h_3 and h_5. We proceed to fit them by demanding that the $B^*\pi$ squared scattering amplitude peaks at the mass of the $B_1(5721)^0$ resonance $[I(J^P) = 1/2(1^+)]$; (5723.5 ± 2.0) MeV [12]. Following the discussion in [8] we can estimate a valid range for h_5 from our results in the D sector. Taking into account that h_5 scales as $h_5 \sim m_D^{-2}$, we use for the B sector:

$$h_5^B = h_5^D \left(\frac{m_D}{m_B}\right)^2 , \tag{26}$$

leading to a value of $h_5 = -0.04$ GeV^{-2}. The value of h_3 does not affect very much the pole position of the resonance.

Choosing a value of $h_3 = 2.5$ we obtain the final result in Fig. 4. The predicted mass for this state from the peak of the amplitude is still about 100 MeV below the $B_1(5721)^0$ mass. We find, as discussed in Appendix A, that it is not possible to fix simultaneously the low energy and subtraction constants –in a natural choice– in

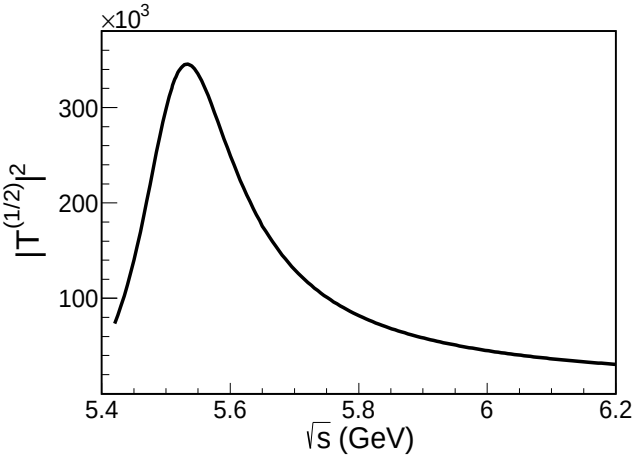

FIG. 2: Square amplitude for $B\pi$ scattering with isospin $I = 1/2$ and at LO in ChPT.

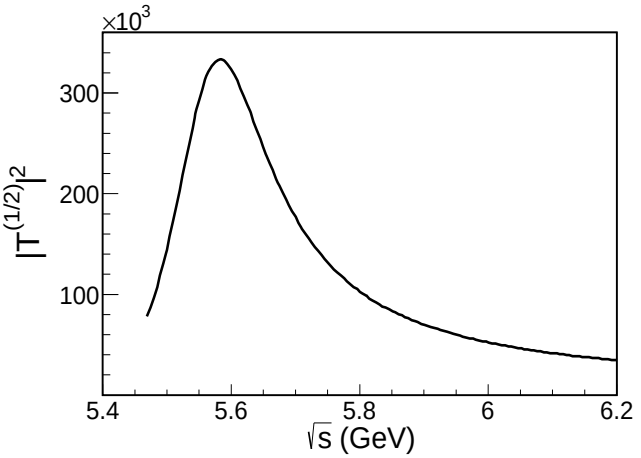

FIG. 3: Square amplitude for $B^*\pi$ scattering with isospin $I = 1/2$ at LO in ChPT, computed replacing m_B by m_B^* in Eq. 17.

order to get values nearer the expected $B_1(5721)$ mass. Furthermore, our findings are in agreement with those in Refs. [13, 14, 16]. Because of the lack of experimental evidence of a B_1 state decaying into $B^*\pi$, the most reasonable choice is to keep the values of the LECs determined above.

For completeness, we also compute $B\pi$ scattering at NLO in ChPT. This channel is also resonant, with $m_{B_0} = 5534$ MeV. Again, there is no data yet at our disposal to compare with. The total cross section for the $B\pi$ channel (considering the two isospin channels $I = 1/2$ and $3/2$) is shown in Fig. 5.

The $I = 1/2$ cross section at threshold is 18.1 mbarn, or equivalently an S-wave scattering lenght of $a_{B\pi}^{1/2} = 0.38$ fm or $m_\pi a_{B_\pi} = 0.26$ is found, in total agreement with the results of [15] but larger than the result of [17], $a_{B\pi}^{1/2} = 0.25$ fm. For the repulsive channel $I = 3/2$ we find a cross section of 1.5 mbarn, or $a_{B\pi}^{3/2} = -0.11$ fm,

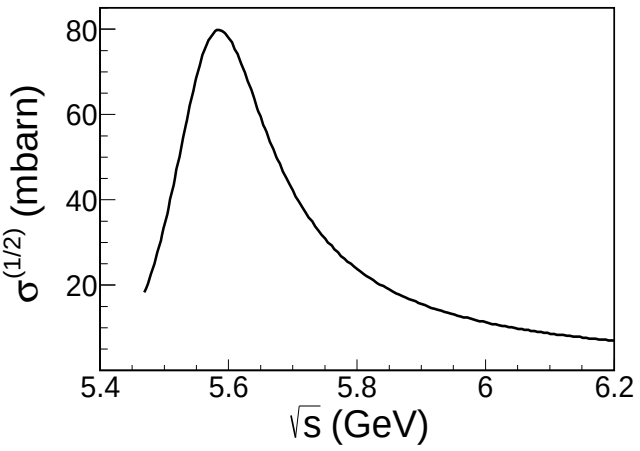

FIG. 4: Cross section for $B^*\pi$ scattering with isospin $I = 1/2$ and at NLO in ChPT, computed replacing m_B by m_B^*, and considering $(h_1, h_3, h_5) = (-1.042, 2.5, -0.04\ \text{GeV}^{-2})$. The resonance is to be understood as the broad B_1.

close to the results in [17] of -0.17 fm.

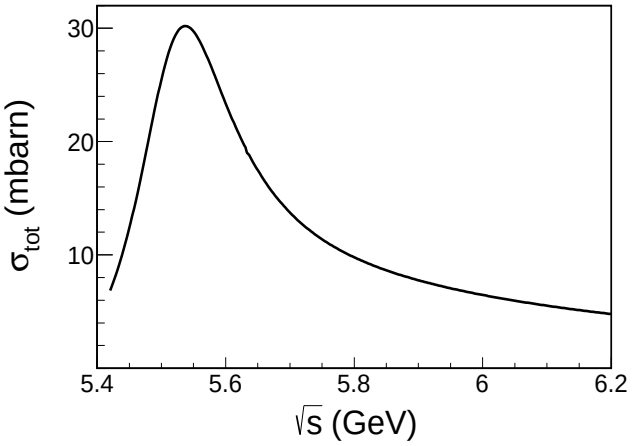

FIG. 5: Total $B\pi$ cross section (both 1/2 and 3/2 isospin channels) at NLO in ChPT, $(h_1, h_3, h_5) = (-1.042, 2.5, -0.04\ \text{GeV}^{-2})$.

After the estimation of the free relevant constants for the $B^{(*)}\phi$ scattering amplitude, we are now in position to compute the transport coefficients, which are the subject of the next section.

IV. DRAG AND DIFFUSION COEFFICIENTS

We proceed to calculate the F, Γ_0 and Γ_1 transport coefficients defined in Eq. (2), for bottomed mesons in a pure pion gas. We expect the contribution of pions to be the most relevant one because of their large multiplicity in comparison to other particles. For completeness, in this work we also account for the effect of the other

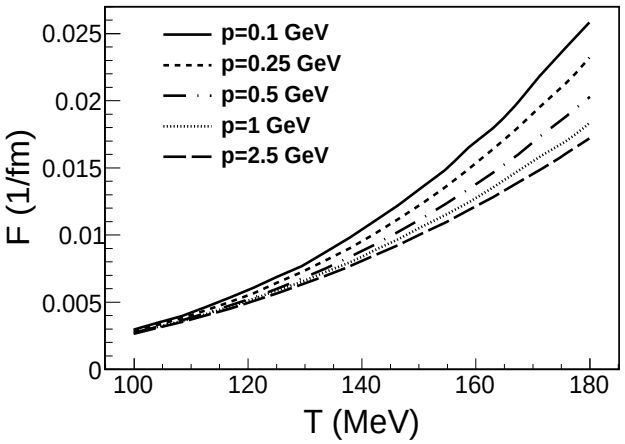

FIG. 6: Momentum-space drag coefficient as function of temperature for several bottom quark momenta in the pion gas.

members of the light meson $SU(3)$ octet. A detailed discussion is done in Section V.

In Fig. 6 we show the dependence on the temperature and B-meson momentum of the drag coefficient F. We observe an increase of a factor of about 6-8 in the range from $T = 100 - 180$ MeV, which means that the temperature evolution of the thermal medium can modify the nature of its interaction with the B-mesons. So, the drag in a heavy-ion collision is considerably strengthened in the hotter stages, with a significant interaction between heavy mesons and thermal medium, and accordingly at larger momentum transfers. However, as the temperature of thermal bath diminishes, the magnitude of interaction decreases and the bottomed mesons move more freely. The drag coefficient exhibits a mild momentum dependence of about 10% in the range $[0.5, 2.5]$ GeV, whereas more pronounced at low p. From this coefficient we estimate the relaxation length of bottom quarks in the hadronic medium. Taking the pion gas at a temperature of 150 MeV (at which our approach is reliable), we find

$$\lambda_B(T = 150 \text{ MeV}, p = 1 \text{ GeV}) = \frac{1}{F} \simeq \frac{1}{0.01} \text{ fm} = 100 \text{ fm} \tag{27}$$

for bottomed mesons travelling with a typical momentum of 1 GeV. This value of λ_B is considerably bigger than the case of charmed mesons, evaluated in the same approach in Ref. [4] (there $\lambda_D \simeq 40$ fm). Thus, it is reasonable to expect that the lifetime of the pion gas (typically 5-10 fm) is smaller than the relaxation time of both D and B mesons, which means that heavy quarks do not completely relax before leaving the hadronic medium.

Another point worthy of mention is that the drag coefficient for charmed mesons computed in our previous work [4] is about three times larger than the one for bottomed mesons at small p. This scaling is the correct one when looking at the non-relativistic expression of this coefficient in the static limit

$$F \simeq \frac{1}{3}\sigma P \sqrt{\frac{m_\pi}{T}} \frac{1}{m_B} \ , \tag{28}$$

where σ is the total cross section and P the pressure of the gas. Note that there is a dependence on the heavy-flavor mass in the denominator. This makes the drag coefficient smaller for heavier mesons. With respect to the D meson system, the drag force is suppresed by a factor of $m_B/m_D \simeq 2.8$ in very good agreement with what we observe in our results. Note that in the low energy limit the cross section does not depend on the heavy meson mass. This is not the case at higher temperatures where Eq. (28) contains further corrections in powers of $1/m_B$. This scaling is also observed for the drag coefficient of b and c quarks in the static limit beyond the critical temperature within the phenomenological approach of Ref. [18, 19], in total accordance with our findings in the hadronic phase. We observe, however, that this scaling is not maintained in the results of [3, 6]. There, a similar approach based on heavy-meson ChPT amplitudes is used to calculate the transport coefficients of D- and B-mesons. However, the authors employ NLO perturbative amplitudes in the case of $D\pi$ scattering [3], overestimating the effect due to the high-energy dependence of their cross sections. This is partly solved in [6] for the B system, where NLO amplitudes at threshold energy (scattering lenghts) are used in the evaluation of B-meson transport, thus taming the high-energy behavior of the amplitudes. In contrast, this approximation underestimates diffusion from resonant scattering in the $B^{(*)}\pi(1/2)$ channel. This discussion reinforces the role of unitarization of low-energy scattering amplitudes to obtain realistic transport coefficients at high temperatures in the heavy-flavor sector. A more detailed discussion of the use of perturbative versus unitarized amplitudes is carried over at the end of this section.

In Fig. 7 the temperature dependence of the B meson diffusion coefficients Γ_0 and Γ_1 is displayed for several momenta. The two coefficients become degenerate in the static limit, $p \to 0$. At $p = 0.1$ GeV this limit is already well reached. Interestingly, one finds that numerically this coefficients are very similar to those obtained for the D meson case in Ref. [4]. Looking at the non-relativistic expression of these coefficients gives a clue for this fact:

$$\Gamma_0, \Gamma_1 \simeq \frac{1}{3}\sigma P \sqrt{m_\pi T} \ , \tag{29}$$

where we have used the Einstein relation

$$F = \frac{\Gamma}{m_B T} \tag{30}$$

to obtain this equation. The coefficients Γ_0 and Γ_1 are independent on the heavy quark mass in the nonrelativistic limit. For this reason the results in Fig. 7 are basically the same as those in Ref. [4]. In Ref. [18, 19] very similar diffusion coefficients are found in the c and b quark

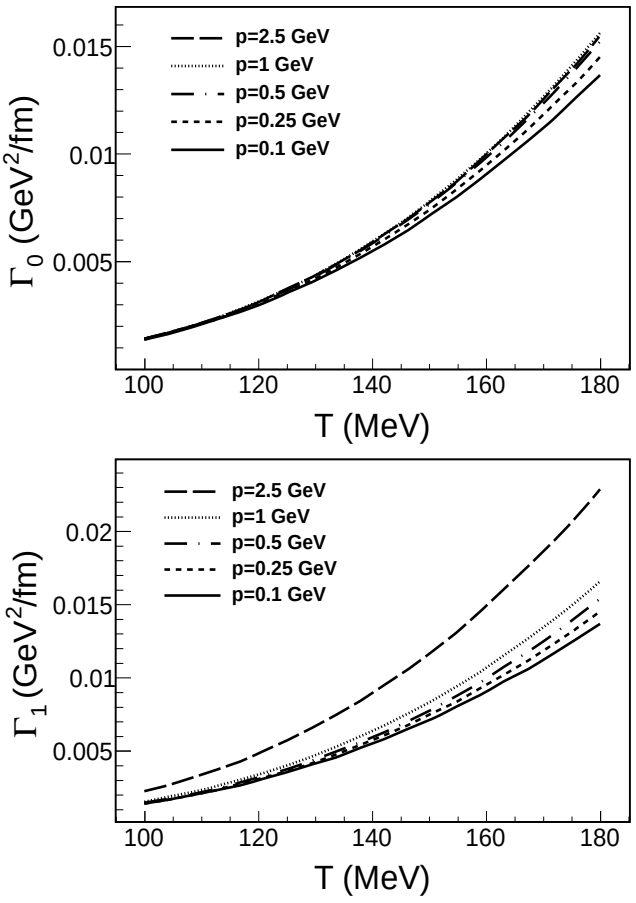

FIG. 7: Momentum-space diffusion coefficients as function of temperature for several bottom quark momenta in the hadron gas.

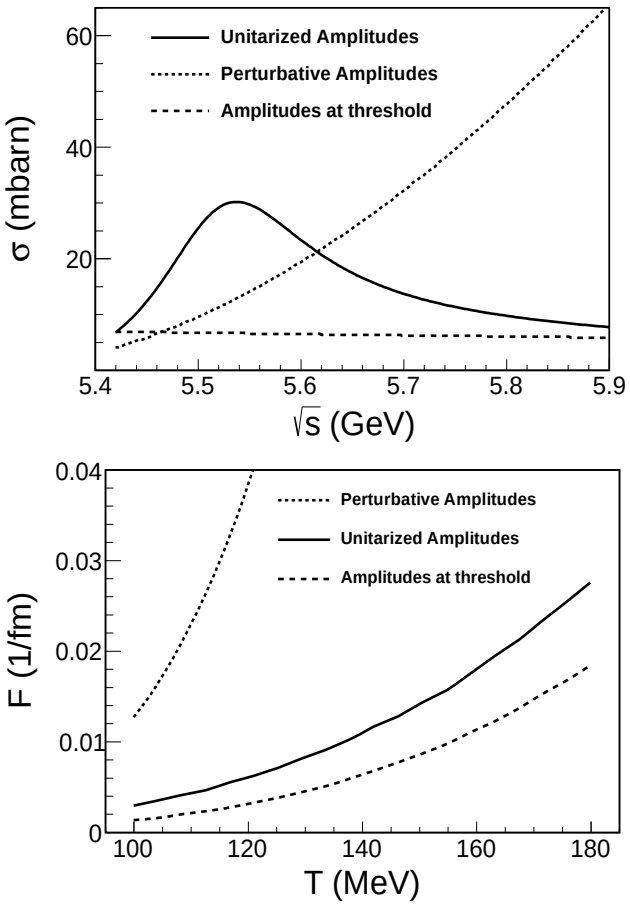

FIG. 8: Upper panel: $B\pi$ isospin averaged total cross section for different choices of the scattering amplitudes: unitarized, perturbative, and scattering lengths. Lower panel: Corresponding drag coefficient in static limit as a function of temperature.

systems, confirming the prediction of the nonrelativistic kinetic theory. These findings constitute an additional consistency test of our calculations.

In the following we study the role of unitarization in obtaining realistic amplitudes for B meson scattering off the light gas and its impact on the transport coefficients. We deem this is an important point in order to understand the wide range of results for transport coefficients that can be found in literature within similar approaches based on effective theories of heavy meson interactions. In Fig. 8 we depict the $B\pi$ total cross section in three different schemes: using NLO (perturbative) chiral amplitudes, unitarized amplitudes as described in Sec. III.B, and NLO amplitudes evaluated at threshold energy (scattering lengths). We observe that the perturbative cross section grows monotonically with energy, as expected from the chiral expansion. The cross section within the threshold approximation is essentially flat over the full energy range. The unitarized cross section, in contrast, peaks at the resonance region, dominating over the other two schemes, whereas later it decreases at higher energies as expected from phase space considerations. The corresponding drag coefficient with $p = 0.1$ GeV is shown in the lower panel of Fig. 8. The perturbative scheme leads to an unrealistic temperature behavior of F, which is clearly tied to the unphysical high-energy behavior of the cross section. The scattering length approach does not suffer from this artifact at high energies. However, it provides a rather smaller diffusion coefficient (factor $1.5-2$) over the whole temperature range as compared to the unitarized scheme, since it misses the s-channel enhancement of the interaction due to the presence of resonances. The unitarized scheme leads to the most realistic result in our opinion, accounting for the phenomenology of the heavy-meson interaction in view of the current knowledge of the B-meson spectrum, and with a controlled high-energy behavior.

Finally, a comment on the Einstein relation within our calculation is in order. In the evaluation of F, Γ_0 and Γ_1 we have not made use of the Einstein relation to obtain the coefficients at low momentum, but performed the calculation explicitly as in Eqs. (2) and (3). A pertinent consistency test can be done by obtaining the diffusion coefficient from the drag coefficient (or viceversa) in

static limit from the Einstein relation. Numerically, the integrations in Eq. (2) have to be performed with a suitable pion momentum cutoff which ensures convergence. One expects the gas distribution function to supress the integrand at large pion momentum beyond the chosen cutoff so that high-energy contributions are negligible. We observe, for instance, that using a cutoff for the pion momentum of about $4\pi F = 1.2$ GeV makes our results sensitive at very high temperatures, where the Einstein relation is not well fulfilled. On the other hand, one cannot increase arbitrarily this cutoff to achieve convergence, as this implies that the scattering amplitudes have to be evaluated at energies which escape the expected validity of the effective theory. Studying how much the static coefficients deviate from fulfilling the Einstein relation as a function of the momentum cutoff can be considered as an estimate of the systematic error in our computation of the transport coefficients. An example of this is provided in Fig. 9. In the upper panel we plot the function F at $p = 0.1$ GeV (very close to the static limit) as obtained from Eqs. (2,3) with a momentum cutoff of 1.2 GeV, together with the determination from Γ_0, Γ_1 using the Einstein relation. The differences are due to the finite pion momentum cutoff. In the lower panel the same curves are shown with a cutoff of 3 GeV. This higher cutoff ensures convergence of the transport integrals at all temperatures and the Einstein relation is well satisfied. It is worth mentioning that the scattering length scheme discussed above ensures a much quicker convergence of the transport integrals, at a cost, however, of implementing an unrealistic energy dependence of the heavy-light meson cross sections and missing the phenomenological information from resonance-enhanced diffusion.

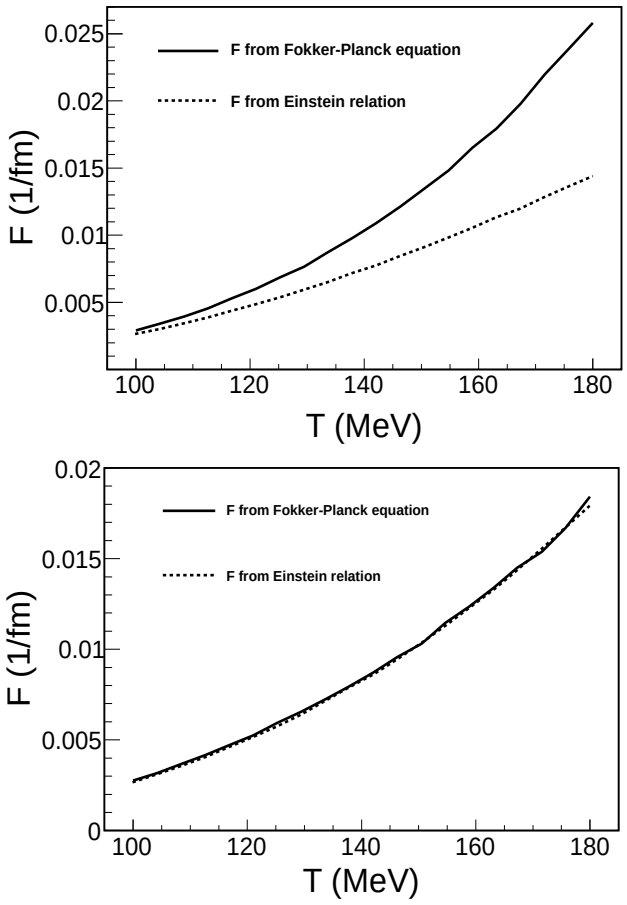

FIG. 9: Upper panel: Drag force at $p = 0.1$ GeV as evaluated from Eq. (2) and (30). The Einstein relation is not satisfied at high temperatures due to the momentum cutoff coming from the effectve theory ($\sqrt{s} \lesssim 6.5$ GeV). Lower panel: Same as above but with a larger cutoff momentum.

V. EFFECT OF KAONS AND η MESONS

Analogously to our previous work, so far we have studied the interaction of the bottomed mesons with pions, as they are most abundant at heavy-ion collision temperatures. However, the mesonic gas is also populated by kaons and η mesons, with whom the heavy mesons can also interact. In Sec. III we only discussed scattering channels involving pions, although we have actually extended the computation to the other members of the $SU(3)$ octet. With this information it is straightforward to implement the contribution from kaons and η's to the transport coefficients. We also added these states for the sake of comparison with other references, particularly [6].

The changes in our calculation are minimal and they affect to the collision rate w defined in Eq. (3), which now reads

$$w = w_\pi + w_K + w_{\overline{K}} + w_\eta \ . \tag{31}$$

We note that the contribution to the transport coefficients from different species in the gas is always additive, so we expect a moderate increase with the inclusion of these new states.

In Fig. 10 we plot the Γ_0 coefficient of B mesons with a momentum $p = 0.1$ GeV, considering the mesonic gas constituted by different particles. We see that the most relevant contribution comes from the pion gas, as expected. Performing a decomposition of individual hadron contributions to Γ_0 at $T = 150$ MeV we observe that pions provide almost 90% of the total, while the next contribution is provided by kaons and (mostly) anti-kaons. The contribution of η mesons is almost negligible, in agreement with the fact that the $B\eta$ interaction vanishes at LO.

In Fig. 11 we compare the value of the F and Γ_0 coefficients at $p = 0.1$ GeV with those of Ref. [6]. It can be noticed that our results are larger than those of [6], where no unitarization is performed. Γ_0, though, exhibits a smoother growth with temperature in our case, actually being overtaken beyond $T \simeq 150$ MeV. We believe that the reason of this discrepancy is the use, in [6], of scattering lengths (valid in principle for very low energies) in the whole energy and temperature range. As discussed above, this will certainty bring an underestimation of the

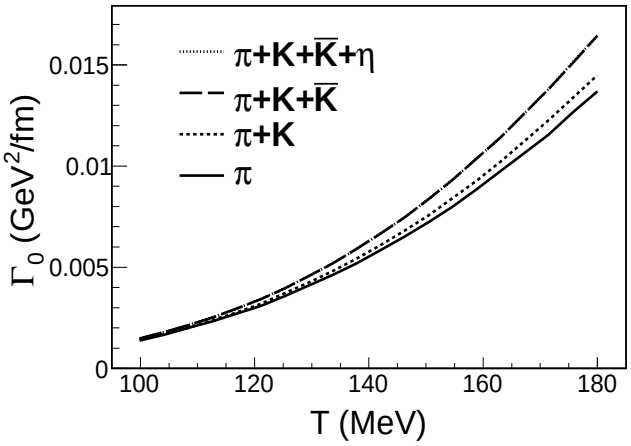

FIG. 10: Γ_0 coefficient of B meson with momentum 0.1 GeV, considering the mesonic gas constituted by different particles.

cross section in the region where resonances take over, producing lower transport coefficients. In contrast, at very high energies, the use of a constant cross section may lead to the opposite effect, explaining the behavior of Γ_0 in the high-temperature region from Ref. [6].

Another point deserving attention is the relaxation of bottom quarks in the present situation, for sake of comparison with that obtained in Section IV, which has been calculated for a pure pion gas. Taking the meson gas at a temperature of 150 MeV, the relaxation length of bottomed mesons travelling with 1 GeV momentum in the full meson gas is

$$\lambda_B(T = 150\ \text{MeV}, p = 1\ \text{GeV}) = \frac{1}{F} \simeq \frac{1}{0.012}\ \text{fm} \simeq 83\ \text{fm}\,, \tag{32}$$

We find that the value for λ_B in Eq. (32) is reduced with respect to that estimated in Eq. (27), since in the present case the inclusion of other contributions to the meson gas yields an increase of the transport coefficients. However, this thermal relaxation time continues greater than the lifetime of hadron gas, allowing us to consider that indeed heavy quarks are carriers of information of the phase transition upon exiting the hadron gas.

For completeness, we also account in Figs. 12 and 13 for the evolution of the transport coefficients and the extracted bottom relaxation length with the heavy-meson momentum, in the full meson gas, at a temperature of 150 MeV.

In the present approach we can also estimate the energy and momentum loss per unit length of a bottomed meson travelling in the meson gas from the classical interpretation of the F coefficient as a drag force. One has

$$dE/dx = -F\,p\,, \quad \text{and} \quad dp/dx = -F\,E\,, \tag{33}$$

in terms of the energy and momentum of the bottomed meson. These quantities are depicted in Fig. 14 at $T =$

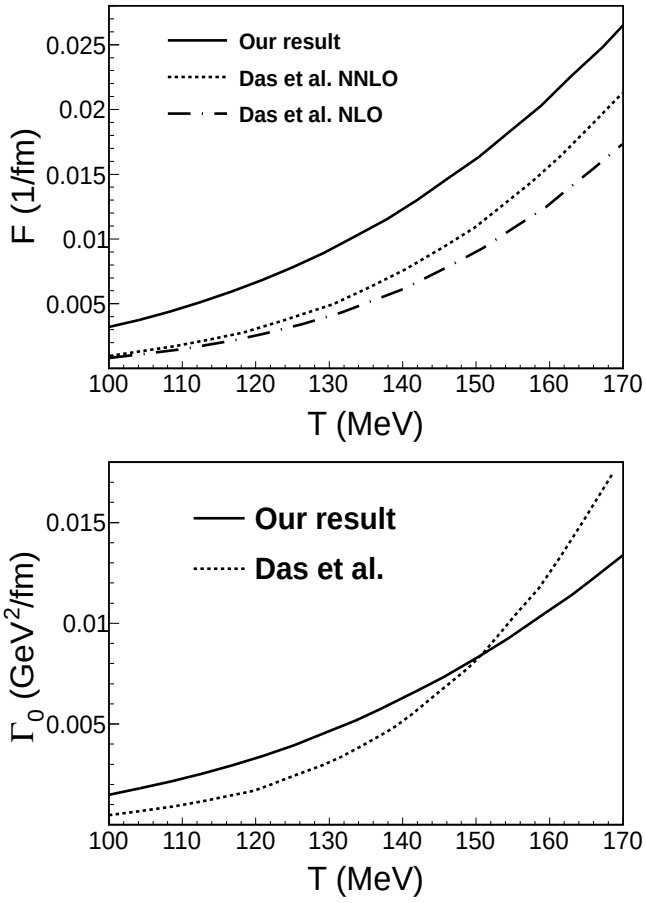

FIG. 11: F and Γ_0 coefficient at $p = 0.1$ GeV in comparison with the results of [6].

150 MeV for the $SU(3)$ meson gas. Thus, a reference bottom quark in a B or B^* mesonic state with a typical momentum of 1 GeV with respect of the rest frame of the surrounding medium, loses about 70 MeV per Fermi as it propagates in the hadron gas. This effect should be taken into account to correctly analyze heavy-meson distributions, suggesting that the hadronic phase also has to be treated in hydrodynamical simulations regarding open heavy flavor probes.

Finally, we calculate the spatial difusion coefficient, D_x, which can be related to the diffusion coefficient in static limit as $D_x = T^2/\Gamma$ (cf. [4], Appendix B for details). It is shown in Fig. 15 together with our previous result for charmed mesons, below the crossover, and with the estimations by Rapp and van Hees for c- and b-quark transport properties above the critical temperature [18–20]. The conclusion observed for the charm sector is here confirmed for bottom: the minimum relaxation time for heavy flavor seems to take place around the crossover, where one expects strongest (and long-range) interactions. Our present work reinforces the use of heavy flavor as probes of the QCD phase transition by reducing theoretical uncertainties regarding the dynamics in

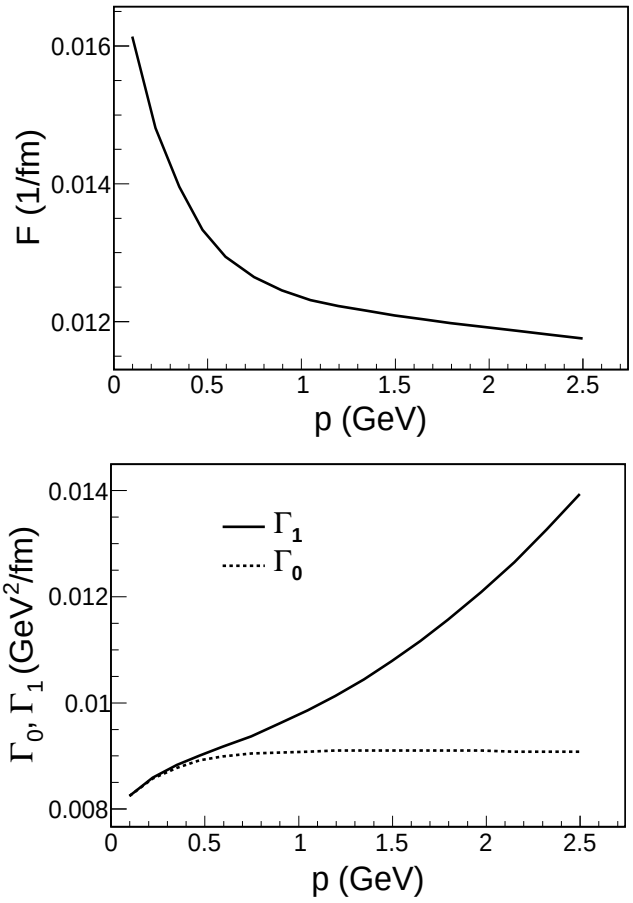

FIG. 12: F (upper panel) and Γ_0, Γ_1 (lower panel) coefficients at $T = 150$ MeV as a function of the heavy-meson momentum.

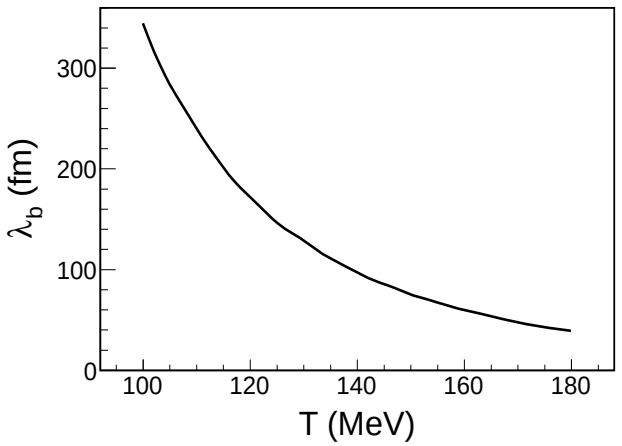

FIG. 13: Bottom relaxation length in the hadronic phase at $p = 0.1$ GeV as a function of the temperature.

the hadronic phase.

VI. SUMMARY AND CONCLUSIONS

In this work the drag and diffusion coefficients of bottomed mesons in a thermal gas of pions, kaons and η mesons have been evaluated in a Fokker-Plank transport approach. The dynamics of the interaction of B and B^* with the light mesons has been modelled employing a unitarized version of heavy-meson chiral perturbation theory within the constraints of heavy quark symmetry. The relevant scattering amplitudes have been calculated at next-to-leading order in the chiral expansion and leading order in the heavy quark limit, and the free parameters have been constrained by available data on the $B^{(*)}$ spectrum and heavy-quark considerations.

We have observed a sizable temperature dependence of the transport coefficients, indicating that both drag and diffusion are more efficient in the hotter stages of the hadronic phase in a heavy-ion collision.

Regarding momentum dependence, it turns out that F and Γ_0 only change mildly whereas transverse coefficient, Γ_1, is particularly sensitive to the momentum of the heavy meson. The latter may lead to observable consequences in the analysis of anisotropic observables such as the elliptic flow.

In addition, a detailed comparison has been accomplished between our outcomes and the other ones in literature obtained via different approaches. Our statements rely on a good control of the elementary B-meson interaction with the light meson octet over a wide range of energies, accounting for dynamical generation of resonances in attractive channels. We have shown that preserving unitarity in the scattering amplitudes plays an esential role to provide realistic estimates of the transport coefficients at high temperatures.

We have performed several consistency tests of our results such as studying the scaling of transport coefficients with the heavy-quark mass and verifying the Einstein relation in the static limit, which were satisfactory.

Moreover, the individual contribution of pions, kaons and η mesons to the transport coefficients have been estimated. The most relevant contribution is lead by the pion gas, as expected, with the next-to-leading contribution being provided by kaons and anti-kaons.

Also, some estimations of relevant quantities have been done directly from the transport coefficients. One example is the bottom relaxation length, which is about 83 fm for bottomed mesons with momenta of 1 GeV and for meson gas at temperature of 150 MeV. It allows us to infer that bottomed mesons barely relax during the lifetime of the hadron gas, unlike charm mesons that, while not relaxing completely, they loose a great deal of memory of the initial state. In this sense, the bottomed mesons constitute an optimal system to characterize the early stages of a relativistic heavy-ion collision. Observables like the nuclear suppresion factor or the elliptic flow can provide clear indications of the system properties and evolution after the nuclear collision.

Furthermore, the computation of the spatial diffusion

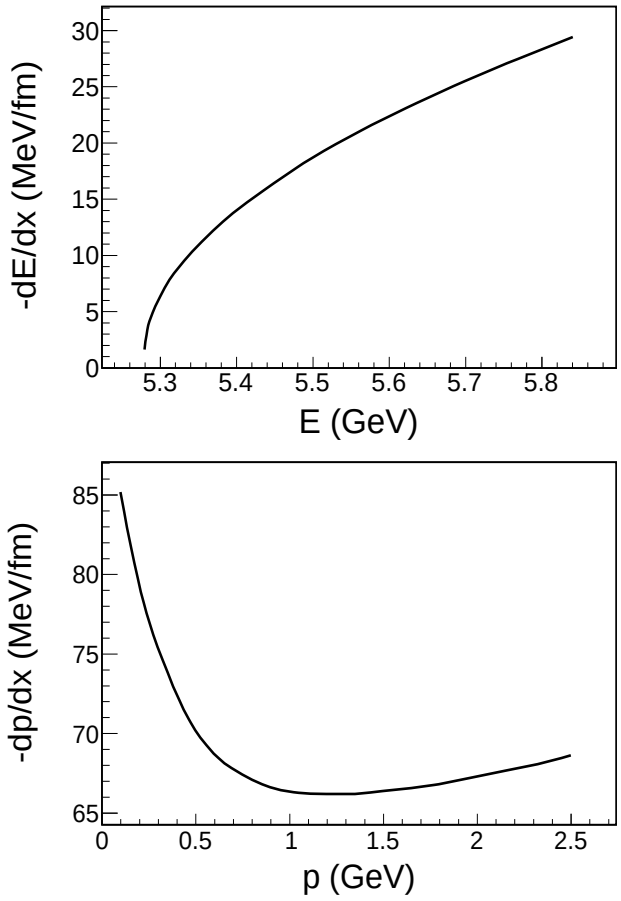

FIG. 14: Energy and momentum loss per unit length of bottomed mesons at a temperature of 150 MeV in the full meson gas consisting of pions, kaons and etas.

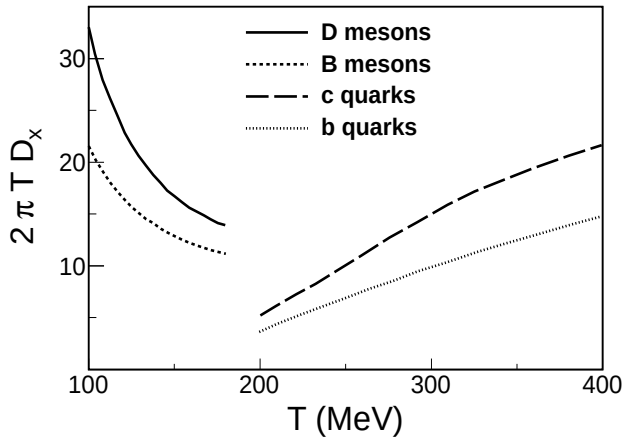

FIG. 15: Charm and bottom spacial diffusion coefficients below (this work) and above ([18–20]) the crossover.

coefficient for the present case is in agreement with the idea that the relaxation time for heavy quarks has a minimum around the crossover to the quark-gluon plasma, the expected place of strongest interactions.

Another interesting quantity evaluated has been the momentum loss per unit length, which is 70 MeV per Fermi for a bottomed meson with momentum of 1 GeV propagating in the hadron gas. This result indicates that to correctly analyze the heavy-meson distributions, the effect of loss of energy and momentum must be taken into account.

Hence, the findings of the present work above discussed reinforce the role of heavy mesons as probes of the strongly interacting matter phase transition, paving the way to a better understanding of heavy-flavor dynamics and transport properties below the crossover.

Acknowledgments

We want to thank Feng-Kun Guo, Juan Nieves, Santosh Ghosh, Christine Davies and Rachel Dowdall for clarifications and comments. We especially acknowledge Felipe J. Llanes-Estrada for invaluable discussions and suggestions.

We thank financial support from grants FPA2011-27853-C02-01, FPA2011-27853-C02-02,FIS2008-01323 (Ministerio de Economía y Competitividad, Spain) and from the EU Integrated Infrastructure Initiative Hadron Physics Project under Grant Agreement n. 227431. LMA thanks CAPES (Brazil) for partial finantial support. DC acknowledges financial support from Centro Nacional de Física de Partículas, Astropartículas y Nuclear (CPAN, Consolider-Ingenio 2010) postdoctoral programme. JMTR is a recipient of an FPU grant (Ministerio de Educación, Cultura y Deporte, Spain).

Appendix A: Subtraction constant

In paralell with the work [4] one would like to provide a reasonable description of meson-meson scattering in such a way that the pertinent resonances in the different channels are generated. In particular, we would like to reproduce the B_0 and B_1 resonances in the $B\pi$ and $B^*\pi$ channels, respectively. However, the masses and widths of these resonances are not yet experimentally known.

Starting at LO, there are no free low energy constants and the perturbative amplitude V in the $B^*\pi$ channel is fixed. In the unitarized amplitude –the one which generates a pole in the amplitude– one introduces a subtraction constant $a(\mu)$. This constant will be fixed by matching the function $G(s)$ in dimensional regularization to the one with cutoff regularization scheme.

The loop function $G(s)$ in dimensional regularization is given in Eq. (19). The regularization scale μ is chosen at a natural scale of 1 GeV [25] In a cutoff regularization one has [21]

$$G^{\Lambda}(s) = \frac{1}{16\pi^2 s}\left\{2i\sqrt{s}q\left(\arctan\frac{s+m_B^2-m_\pi^2}{2i\sqrt{s}q\sqrt{1+\frac{m_B^2}{\Lambda^2}}}+\arctan\frac{s-m_B^2+m_\pi^2}{2i\sqrt{s}q\sqrt{1+\frac{m_\pi^2}{\Lambda^2}}}\right)\right.$$
$$\left. - \left[(s+m_B^2-m_\pi^2)\log\left(\frac{\Lambda}{m_B}+\sqrt{1+\frac{\Lambda^2}{m_B^2}}\right)+(s-m_B^2+m_\pi^2)\log\left(\frac{\Lambda}{m_\pi}+\sqrt{1+\frac{\Lambda^2}{m_\pi^2}}\right)\right]\right\} . \quad \text{(A1)}$$

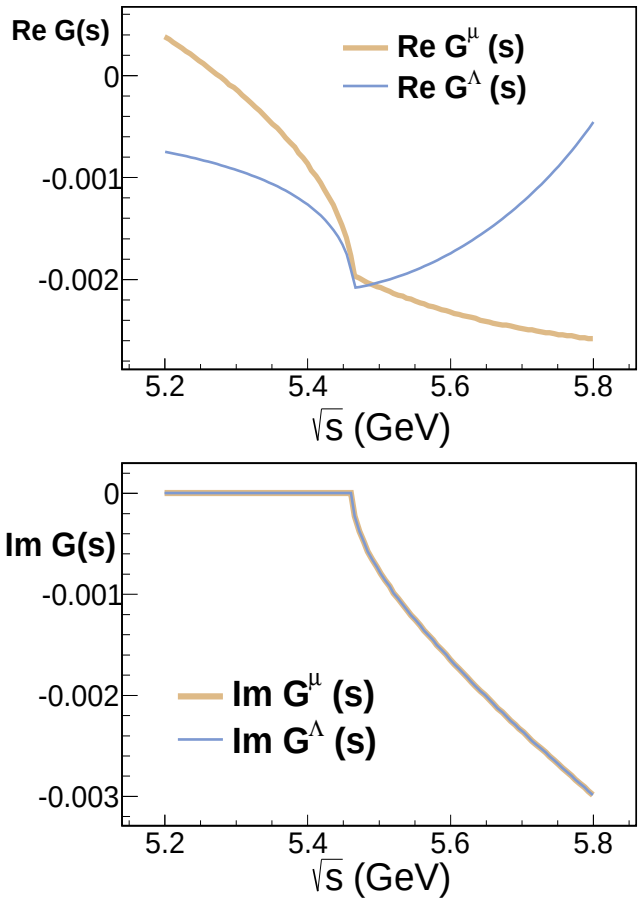

FIG. 16: Re $G(s)$ and Im $G(s)$ from Eq. (19) (dimensional regularization) and Eq. (A1) (cutoff regularization). We match the loop function in the two regularization schemes at $\sqrt{s_{th}} = m_B + m_\pi$. A higher energies $G^{\Lambda}(s)$ becomes non-physical and diverges around $\sqrt{s_\infty} = 6$ GeV.

Note that this expression is valid below and above threshold. The equivalent cutoff in momentum, Λ, is obtained by matching both expressions where we use the value of $a(\mu)$ in the $D\pi$ sector [4]. It is well known that G_Λ presents a spurious divergence at some s_∞ above threshold, where its determination is unreliable. For this reason, one typically compares the two loop functions at threshold $s_{th} = (m_B + m_\pi)^2$ (see Fig. 16).

Combining all these requirements we obtain $a(1\text{ GeV}) = -3.47$, corresponding to a reasonable cutoff momentum of about 1 GeV. Within this scheme we obtain a resonance around 5580 MeV at LO in the $I = 1/2$ channel, about 100 MeV below the reference value of the mass of the B_1 (heavy quark spin 3/2). At NLO the two free low energy constants h_3 and h_5 can modify the pole position and width. Varying these parameters within the constraints of HQ Symmetry, a maximal value of 5587 MeV can be found for the pole position, with a width around 245 MeV. Although higher values of the resonance mass can be forced by tuning the subtraction constant, in order to keep the equivalent cutoff of natural scale we content ourselves with a B_1 pole mass of 5587 MeV and 5534 MeV for the B_0 resonance (with a width of 210 MeV). Our results agree with previous studies using similar unitarization methods. They are summarized in Table III.

[1] M. Laine, JHEP **1104**, 124 (2011) [arXiv:1103.0372 [hep-ph]].

[2] M. He, R. J. Fries and R. Rapp, Phys. Lett. B **701**, 445 (2011) [arXiv:1103.6279 [nucl-th]].

Reference	$M(B_0)$ (MeV)	$\Gamma(B_0)$ (MeV)	$M(B_1)$ (MeV)	$\Gamma(B_1)$ (MeV)
This work	5534	210	5587	245
[14]	5536 ± 29	234 ± 86	-	-
[16]	-	-	5581 ± 5	220 ± 15
[13]	5526	-	5590	-
[15]	5600	-	-	-
[22],[23]	5630 ± 83	-	5693 ± 43	-

TABLE III: Resonance parameters obtained in different works. The last entry corresponds to our estimate from the data given in [22] and [23]. In this case, there is an uncertainty due to the coupling to decay channels which is not included in the quoted error. This uncertainty would presumably increase the error bar in more than 25 MeV.

[3] S. Ghosh, S. KDas, S. Sarkar and J. -eAlam, Phys. Rev. D **84**, 011503 (2011) [arXiv:1104.0163 [nucl-th]].

[4] L. M. Abreu, D. Cabrera, F. J. Llanes-Estrada and J. M. Torres-Rincon, Annals Phys. **326**, 2737 (2011) [arXiv:1104.3815 [hep-ph]].

[5] M. He, R. J. Fries and R. Rapp, Phys. Rev. C **86** (2012) 014903 [arXiv:1106.6006 [nucl-th]].

[6] S. K. Das, S. Ghosh, S. Sarkar and J. -eAlam, Phys. Rev. D **85**, 074017 (2012) [arXiv:1109.3359 [hep-ph]].

[7] M. F. M. Lutz and M. Soyeur, Nucl. Phys. A **813**, 14 (2008) [arXiv:0710.1545 [hep-ph]].

[8] F. -K. Guo, C. Hanhart and U. -G. Meissner, Eur. Phys. J. A **40**, 171 (2009) [arXiv:0901.1597 [hep-ph]].

[9] L. S. Geng, N. Kaiser, J. Martin-Camalich and W. Weise, Phys. Rev. D **82**, 054022 (2010) [arXiv:1008.0383 [hep-ph]].

[10] G. 't Hooft, Nucl. Phys. B **72**, 461 (1974).

[11] L. Roca, E. Oset and J. Singh, Phys. Rev. D **72**, 014002 (2005) [hep-ph/0503273].

[12] J. Beringer *et al.* [Particle Data Group Collaboration], Phys. Rev. D **86**, 010001 (2012).

[13] E. E. Kolomeitsev and M. F. M. Lutz, Phys. Lett. B **582**, 39 (2004) [hep-ph/0307133].

[14] F. -K. Guo, P. -N. Shen, H. -C. Chiang, R. -G. Ping and B. -S. Zou, Phys. Lett. B **641**, 278 (2006) [hep-ph/0603072].

[15] J. M. Flynn and J. Nieves, Phys. Rev. D **75**, 074024 (2007) [hep-ph/0703047].

[16] F. -K. Guo, P. -N. Shen and H. -C. Chiang, Phys. Lett. B **647**, 133 (2007) [hep-ph/0610008].

[17] Y. -R. Liu, X. Liu and S. -L. Zhu, Phys. Rev. D **79**, 094026 (2009) [arXiv:0904.1770 [hep-ph]].

[18] R. Rapp, H. van Hees, [arXiv:0803.0901 [hep-ph]].

[19] H. van Hees, M. Mannarelli, V. Greco and R. Rapp, Phys. Rev. Lett. **100**, 192301 (2008) [arXiv:0709.2884 [hep-ph]].

[20] M. He, R. J. Fries and R. Rapp, arXiv:1204.4442 [nucl-th].

[21] F. -K. Guo, R. -G. Ping, P. -N. Shen, H. -C. Chiang and B. -S. Zou, Nucl. Phys. A **773**, 78 (2006). [hep-ph/0509050].

[22] E. B. Gregory, C. T. H. Davies, I. D. Kendall, J. Koponen, K. Wong, E. Follana, E. Gamiz and G. P. Lepage *et al.*, Phys. Rev. D **83**, 014506 (2011) [arXiv:1010.3848 [hep-lat]].

[23] R. J. Dowdall, C. T. H. Davies, T. C. Hammant and R. R. Horgan, arXiv:1207.5149 [hep-lat].

[24] For a detailed discussion of similar processes involving charmed mesons, see Ref. [4].

[25] There are two typos in [4]. The regularization scale μ should read 1 GeV and $a(1\ \mathrm{GeV}) = -1.85$.